Light beam induced current and infrared thermography studies of multicrystalline silicon solar cells

2004 J. Phys.: Condens. Matter 16 S9

(http://iopscience.iop.org/0953-8984/16/2/002)

INSTITUTE OF PHYSICS PUBLISHING JOURNAL OF PHYSICS: CONDENSED MATTER

J. Phys.: Condens. Matter **16** (2004) S9–S18 PII: S0953-8984(04)66991-8

Light beam induced current and infrared thermography studies of multicrystalline silicon solar cells

A Kaminski[1], O Breitenstein[2], J P Boyeaux[2], P Rakotoniaina[1] and A Laugier[1]

[1] Laboratoire de Physique de la Matière, UMR 5511, Bâtiment Blaise Pascal, Institut National des Sciences Appliquées de Lyon, 7 avenue Jean Capelle, 69621 Villeurbanne Cedex, France

[2] Max Planck Institute of Microstructure Physics, Weinberg 2, D-06120 Halle, Germany

Received 31 July 2003
Published 22 December 2003
Online at stacks.iop.org/JPhysCM/16/S9 (DOI: 10.1088/0953-8984/16/2/002)

Abstract

In this paper we demonstrate the parallel application of light beam induced current (LBIC) and lock-in infrared thermography for the investigation of strong shunting regions in multicrystalline silicon solar cells. Usually both mappings are not correlated, but in this case the shunts could be imaged by both techniques. If for a locally generated photocurrent the conductance through a shunt lying nearby is comparable to that across the emitter into the current amplifier, local shunts become visible in the LBIC as dark regions. After the rear contact of the cell was removed, the LBIC technique was performed from the rear side of the cell. The images point to the existence of inversion layers along grain boundaries crossing the bulk of the cell. Obviously, these inversion layers represent the dominant material-induced shunt type in multicrystalline silicon solar cells. Moreover, it has been shown that cracks may lead to shunts.

(Some figures in this article are in colour only in the electronic version)

1. Introduction

Industrial solar cells are large-area junctions, the performance, lifetime and reliability of which depend strongly on structural and processing-induced defects. Therefore, the photovoltaic industry needs non-destructive techniques permitting the mapping and detection of local defects in large-area solar cells. These defects may be sites of excessive recombination, like grain boundaries or dislocations, or shunts being characterized by an increase of the local dark current. While recombination defects mainly degrade the short circuit current I_{SC} of the cells, shunts mainly degrade the fill factor FF and the open circuit voltage V_{OC} [1].

Several techniques have been proposed to locate recombination defects and shunts in solar cells. EBIC (electron beam induced current) and LBIC (light beam induced current)

techniques measure the variation of the induced current under local electron or photon beam excitation at the surface of the solar cell. Usually, they permit the detection of current variations due to recombinative defects causing diffusion length variations. The advantages of LBIC against EBIC are that it allows the imaging of large-area samples like solar cells and that the penetration depth of the radiation is larger; its disadvantage is that its spatial resolution is worse. Since EBIC and LBIC are performed at zero bias under short circuit conditions, the dark I–V characteristic of the sample does not influence the result, as long as the sample is not heavily shunted (see below). On the other hand, it is much more complicated to image shunts, representing local variations of the dark I–V characteristic, since all local positions in the cell are electrically switched in parallel. It has been proposed to divide solar cells into small mesa diodes by etching techniques and to investigate these diodes separately [2], but this is a very time-consuming, expensive, and destructive approach. The PRAMP (parallel resistance analysis by mapping of potential) technique measures the emitter potential of a biased solar cell in the dark by a probe that mechanically scans the top surface [3]. A shunt is detected by a decrease of the local emitter potential. The drawback of this technique is that it 'scratches' across the surface, and it cannot detect defects under metallization lines, where shunts may be most dangerous. In order to overcome this problem, shunts may be detected thermographically. For example, liquid crystals can be applied on the surface of a biased solar cell in the dark and viewed through crossed polarizers in order to reveal 'hot spots' in positions where the dominant current flows [4]. A more simple version of this investigation is to cover the cell with commercially available sheets made from thermochromic liquid crystals, which under ordinary illumination change their colour when heated [5]. However, the sensitivity of this technique is only sufficient to see shunts under relatively large reverse bias. Note that under operation solar cells are biased at about 0.5 V in the forward direction, so shunts acting under these conditions are the most interesting to study. The first successful non-destructive shunt investigations under forward bias succeeded by using a sensitive thermal sensor, scanning the pulse-biased cell in tipping mode and using lock-in signal treatment (DPCT: dynamic precision contact thermography [6]). However, this technique also necessitates contact between the cell and the thermal sensor, and it requires a long measurement time of many hours. In contrast, infrared thermography (IRT) allows the mapping of temperature without any contact and with a much shorter measurement time than DPCT. It was first applied by Simo and Martinuzzi [7] for shunt imaging, but there again the sensitivity was only sufficient to image shunts under reverse bias, but not good enough for forward bias investigations. Kaminski *et al* [8] have improved the sensitivity of their thermocamera of about 100 mK by a factor of 20 by averaging 1000 images taken with the biased cell and subtracting the average of 1000 images taken without bias. But also there only strong shunts were visible under forward bias. Moreover, these investigations clearly revealed the major problem of all steady-state thermography investigations on silicon solar cells, which is the degradation of the effective spatial resolution caused by the strong lateral heat conductivity of silicon. If heat is locally generated in a silicon cell, this heat instantly tends to spread laterally across an area of the order of 1 cm^2, thus leading to a 'blurred' appearance of steady-state thermographic images of silicon solar cells showing a poor effective spatial resolution.

Both the sensitivity and the effective spatial resolution of thermographic investigations can be greatly improved if they are carried out not in steady-state but in lock-in mode, as was done already for DPCT [6]. Meanwhile lock-in IRT is the most successful technique for shunt investigations on solar cells, also allowing the ability to perform quantitative investigations like non-destructive local I–V characteristic measurements [9–12]. Since temperature and induced current mappings are complementary techniques with respect to their physical interpretation, in this paper first we detail the physical basics of both techniques leading to their different

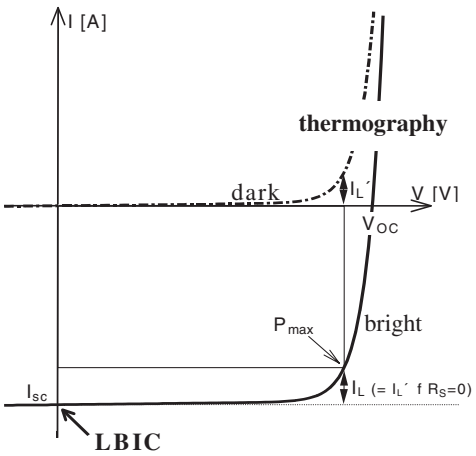

Figure 1. Dark and illuminated (bright) I–V characteristics of a solar cell (qualitatively).

points of view. Then, after introducing the experimental set-ups used for these investigations, the parallel application of both techniques is demonstrated on different multicrystalline solar cells containing both weak and strong shunts. By performing LBIC also on the rear side of a cell with the base contact layer removed, hints to the physical nature of the strongest material-induced shunts could be revealed.

2. Physical basics: LBIC versus IRT on solar cells

For silicon solar cells the so-called superposition principle holds to a good approximation, saying that the illuminated (bright) I–V characteristic equals the dark characteristic parallel shifted by the short circuit current I_{SC}. This principle, which is illustrated in figure 1, comes from the fact that the photo-induced current is nearly independent of the bias of the cell. Note that the photocurrent is always a reverse current, thereby compensating the dark forward current. Hence, under short circuit conditions at zero bias, where the dark forward current is zero, only $-I_{SC}$ is flowing, whereas under open circuit conditions $-I_{SC}$ is just compensated by the dark forward current flowing, and the open circuit voltage V_{OC} is established. Under both conditions the power generated by the cell is zero.

LBIC usually works under short circuit conditions, as indicated by the arrow in figure 1. Therefore its result should not be influenced by the dark I–V characteristic of the cell, as long as series resistance effects can be neglected (see below). If the illuminated cell is electrically loaded, at a certain load the generated power is a maximum. The area of the rectangle inscribed in the bright characteristic in figure 1 is proportional to this power, P_{max}. At the maximum power point the generated current is smaller than I_{SC} by a loss current I_L, and also the generated voltage is smaller than V_{OC}. This is described by the so-called fill factor of the cell given by $FF = P_{max}/(I_{SC}V_{OC})$, which is always smaller than 1 and strongly governs the efficiency of the cell. The steeper the dark I–V characteristic is, the larger is the fill factor and thereby the efficiency. Owing to the superposition principle, the loss current I_L can also be measured as the dark forward current I_L' without illumination at the bias of the maximum power point. This is the base of thermographic shunt investigations. Here the operation of the illuminated cell is simulated by applying the forward bias in the dark (approximately 0.5 V for the maximum power point), whereby the image of the dark forward current can be interpreted as an image

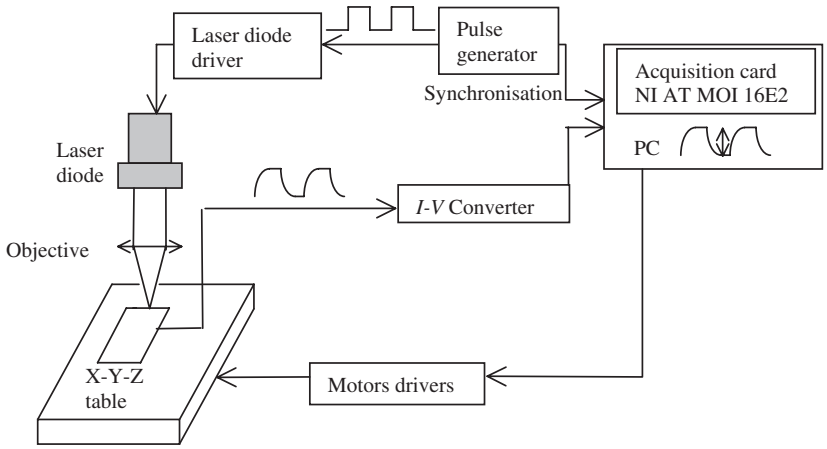

Figure 2. The LBIC set-up used in this work.

of the local loss current also flowing under illumination of the cell. It should be noted that this equivalence holds quantitatively only if series resistance effects can be neglected, which is usually true as long as $I_L \ll I_{SC}$ holds.

3. Experimental details

The solar cells investigated were 12.5×12.5 cm^2 multicrystalline solar cells fabricated using screen-printing technology by an industrial producer. For investigating especially strong shunts, one off-specification cell was also selected. The LBIC- and the lock-in IRT set-ups used for this investigation will be described in the following sections. For performing the LBIC investigation from the rear side, in some regions the Al back contact was dissolved using concentrated HCl, followed by a subsequent removal of the highly p-doped contact region by HF/HNO_3.

3.1. LBIC set-up

In the LBIC set-up (figure 2) [13], the light beam source is a collimated GaAlAs laser diode (780 nm, maximum power: 5 mW) focused by diffraction limited optics. The depth of field of the incident beam is 100 μm and the spot diameter is about 18 μm. The laser diode is used in a modulated mode (typically 100 μs pulse duration and 200 μs repetition time). The laser diode power is measured with a calibrated pin diode: a typical value is about 900 μW which, associated with the 18 μm spot, ensures low injection conditions. It is possible to have a smaller spot by changing the optics, but for large area solar cells a larger spot is preferable for maintaining low injection conditions and for a complete coverage of the area. The tested device is moved under the fixed laser beam on computer-controlled X, Y translation stages (resolution: 1 μm, maximum translation: 75 mm). The photogenerated current is measured by an I–V converter and sent to an acquisition card. The numerical photocurrent or photovoltage value for each point with and without light is averaged to get a good signal/noise ratio and the values with and without light are subtracted. The associated value is stored in a data file, together with all relevant measurement parameters. A typical map obtained with this apparatus contains 250×250 points with a step width of 100 μm. This 2.5×2.5 cm^2 map is performed in about 7 h, the main time limiting factor being the X–Y table displacement speed and the necessary averaging of the signal for strongly shunted solar cells.

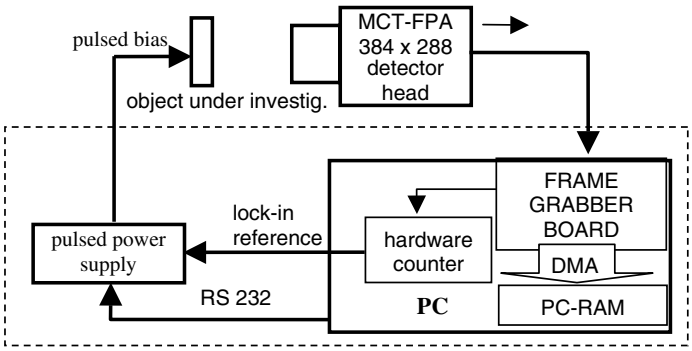

Figure 3. Schematic diagram of the TDL 384 M 'Lock-in' thermography system.

3.2. Lock-in IRT set-up

The lock-in IRT results have been obtained using the commercial TDL 384 M 'Lock-in' system, which is available from Thermosensorik GmbH Erlangen/Germany [14]. Figure 3 shows the scheme of this system, which is based on a development of MPI Halle [9]. The system uses a mercury–cadmium-telluride (MCT) focal plane array (FPA) IR detector head made by AIM Heilbronn/Germany, which has a resolution of 384 × 288 pixel, detects in the mid-IR range (3–5 μm), and has a nominal sensitivity of about 25 mK. The maximum full frame rate is 120 Hz; if only 288 × 288 pixel are used the frame rate increases to 160 Hz. The system is controlled by a PC running under Windows NT, which, by using a frame grabber board and direct memory access (DMA), writes the incoming frames cyclically into a certain range of the RAM, where they are picked up by the processor for evaluation. Details of the lock-in correlation procedure were presented elsewhere [12]. A hardware counter, which is directly controlled by the frame trigger of the camera, is used for generating the bias pulse trigger signal (lock-in reference), which controls a pulsed power supply. The pulsed bias is fed to the object under investigation, where in positions of local heat sources the surface temperature is periodically modulated. The lock-in correlation procedure converts the incoming images into an image of the local temperature modulation amplitude. By averaging over many periods the noise level reduces with $1/\sqrt{t_{\text{acquisition}}}$, reaching a level below 100 μK after an acquisition time above 10 min [9]. Hence, lock-in thermography allows us to image not only strong but also very weak shunts, and even the homogeneous heating of the cell caused by the homogeneously flowing forward current. The IR camera may be equipped with different IR objectives, whereby a special microscope objective leads to a pixel resolution below 10 μm [15].

Note that one common source of inaccuracy of IRT is the IR emissivity of the imaged surface, which is the probability of a surface to emit IR radiation at a certain temperature. The IR emissivity of a surface equals its absorbance at this wavelength, which is known as Kirchhoff's law. Especially reflecting surfaces like that of the grid metallization of solar cells show a low IR absorption and therefore a low IR emissivity. Hence, if there were heat sources below grid lines, they might remain invisible owing to the low emissivity of this surface. In our system this problem is avoided by covering the cell with a 20 μm thin blackened plastic film, which is sucked against the sample by a vacuum and serves as an efficient IR emitter.

4. Results

A comparison of LBIC and lock-in IRT images of a typical multicrystalline silicon solar cell having only weak shunts ($R_{\text{sh}} = 12\ \text{k}\Omega\,\text{cm}^2$) is shown in figure 4. In order to

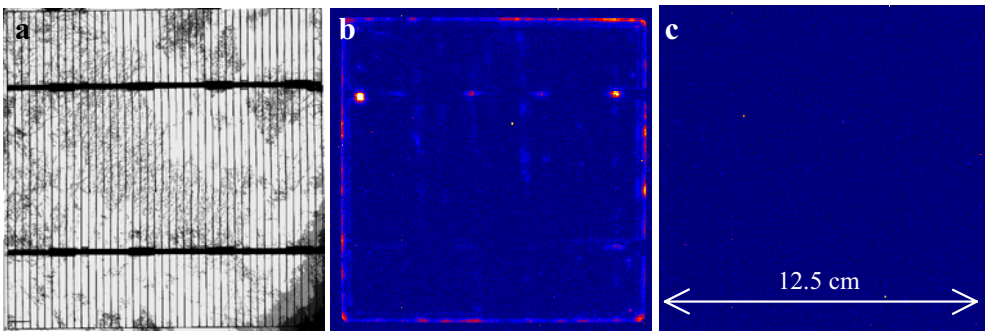

Figure 4. LBIC image (step: 150 μm, distance between two metallization lines: 2.9 mm) (a), lock-in thermogram measured at +0.5 V forward bias (b), and lock-in thermogram measured at -0.5 V reverse bias (c) of a typical 12.5 $\times$ 12.5 cm^2 multicrystalline silicon solar cell.

distinguish between ohmic shunts and shunts having a diode-like I–V characteristic, two lock-in thermograms measured at 13 Hz are shown, one measured at +0.5 V forward bias and one measured at -0.5 V reverse bias. Both thermograms are scaled to the same maximum brightness of 1 mK T-modulation amplitude. If only one shunt were visible with the same brightness in both thermograms, it would show an ohmic (linear) I–V characteristic. In the LBIC image (a) the crystal structure of the cell is clearly visible; hence grain boundaries are visible as dark lines. This is the expected behaviour: if the light beam irradiates the cell in the vicinity of a grain boundary, some part of the generated minority carriers recombine at the grain boundary states, leading to a locally reduced number of carriers collected by the pn-junction there. Also the metallic current collection grid at the surface of the cell is clearly visible. This is a simple shadow effect: the exciting light is not able to penetrate the grid metallization. A relative photocurrent decrease of 15% is observed at the bottom right corner. This can be due to a variation of the reflectivity or of the minority diffusion length. On the other hand, neither the grain boundaries nor the grid lines are visible in the thermograms. Instead, the forward bias thermogram shows some shunts at the edge of the cell (edge shunts), and some shunts at the position of the major (horizontal) grid lines. Interestingly, none of these shunts is visible under reverse bias, hence all of them show a nonlinear (diode-like) I–V characteristic. Also this is a typical behaviour for this kind of solar cells. At the edge of the cell the pn-junction comes to the surface. If there are any surface recombination states there, they will lead to local recombination currents in these positions, which are indeed expected to flow only under forward bias. The nonlinear shunts below the grid lines may have a different origin. Note that the n-doped emitter layer at the top of the cell has a thickness of only 0.3 μm. If for any reason the grid metal is in direct contact with the silicon p-base material, this would lead to so-called 'Schottky type' shunts, which are also characterized by a diode-like I–V characteristic. The metallization thickness is about 10 μm, which is thin enough that the thermal waves easily penetrate the metallization without any remarkable attenuation. The recombination action of the grain boundaries is obviously not strong enough to lead to sufficiently strong local recombination currents as in the case of the edge shunts. Thus, there is virtually no correlation between the LBIC and lock-in IRT visible in figure 4. This points to the complementary information that can be gained from LBIC and lock-in IRT investigations: LBIC displays inhomogeneities of the local short circuit current I_{SC}, which is not influenced by the dark I–V characteristic. On the other hand, lock-in IRT displays inhomogeneities of the dark I–V characteristic, which basically influences the fill factor FF and the open circuit

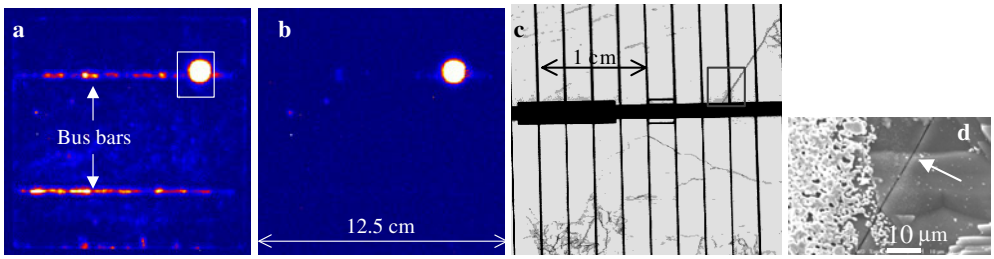

Figure 5. (a) Lock-in thermogram measured at +0.5 V forward bias, and (b) lock-in thermogram measured at −0.5 V reverse bias of a 12.5 × 12.5 cm^2 multicrystalline silicon solar cell having a strong ohmic shunt, and (c) LBIC image (step: 100 μm, $\Delta I/I_{\mathrm{LBICmax}} = 20\%$) of the shunt area in the white rectangle in figure (a). The black rectangle in figure (c) indicates the supposed position of the shunt. (d) SEM image of the central region of the black rectangle in figure (c); the arrow indicates the crack.

voltage V_{OC} of the cell. Thus, in order to characterize the inhomogeneity of all three quality parameters of solar cells, I_{SC}, FF, and V_{OC}, one needs to apply both techniques as demonstrated here.

Figure 5 shows the same sets of images for a cell showing a larger recombination current and a lower ohmic shunt resistance (230 Ω cm^2). Here the nonlinear Schottky-type shunts below the grid lines are considerably stronger than in figure 4, and additionally there is a strong linear (ohmic) shunt having the same brightness under forward and under reverse bias. Actually, this shunt is only a small bright point, but its thermal signal is larger than that of the other shunts by a factor of about 200. Since the scaling was chosen here similarly to that of figure 4, this defect appears artificially broadened due to the lateral heat diffusion in the silicon material. If the thermogram had been shown scaled to clearly show this defect, the other defects would have been invisible. In the LBIC image (c), at the position of the hot spot detected by IRT, a dark line is crossing a grid line and the bus bar metallization. SEM investigations (figure 5(d)) permit us to demonstrate that this dark line is not a grain boundary but a crack. Obviously during screen printing metal paste has penetrated this crack, thus producing a strong metallic shunt between the grid line and the rear contact. This shunt is not visible in the LBIC.

As a final example, figure 6 shows three LBIC images and one lock-in thermogram of a region of an off-specification solar cell, which was very strongly shunted (shunt resistance less than 160 Ω cm^2). The network-like shunting system visible in the forward bias thermogram (a) was also visible under reverse bias; hence these are all ohmic shunts. In the LBIC image (b) these shunts were also visible as a cloudy dark contrast. Hence, unexpectedly here we see a clear correlation between LBIC and lock-in IRT, which will be explained in the following section. It was suspected that these shunts might be due to inversion layers along grain boundaries which are crossing the wafer material and short-circuiting the emitter with back metallization. In order to prove this hypothesis, the rear contact of the cell and the highly doped p^+ contact layer (also called back surface field/BSF layer) were chemically removed in the shunt region, and LBIC was performed from the rear side of the cell. In the absence of inversion layers, grain boundaries would in this geometry also lead to dark LBIC contrast. However, if inversion layers are present, they show a bright contrast, since they represent preferred conducting channels towards the emitter for the photogenerated carriers. The result of the LBIC investigation from the rear in the region framed in figure 6(b) is shown in 6(c). Here we clearly see bright lines, which correlate with the positions of grain boundaries. This is a clear proof of the existence of

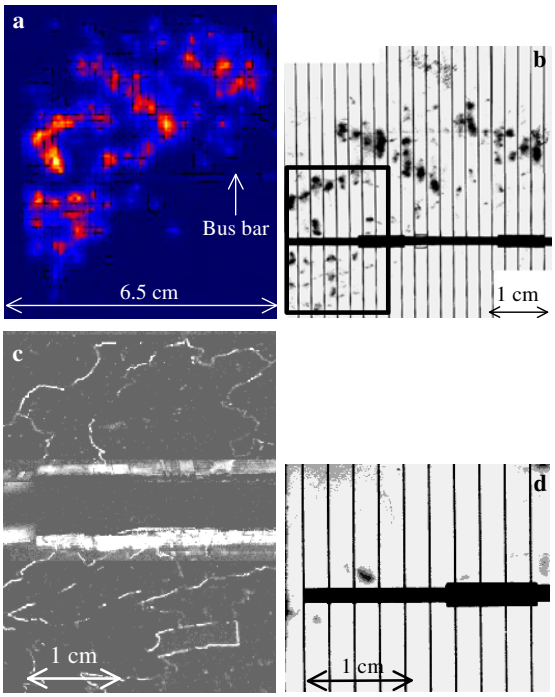

Figure 6. (a) Lock-in thermogram under 0.5 V forward bias, (b) LBIC image (step size: 100 μm), (c) LBIC image (step: 100 μm) of the regions framed in (b), measured after removing the rear contact from the rear side of the cell, and (d) LBIC image of nearly the same area measured on the front side of the cell.

inversion layers crossing the cell. Moreover, on the LBIC image performed on the front side of the cell after etching away the back contact (figure 6(d)), the cloudy defects are no longer visible except near the bus bar. This is probably because the BSF was only incompletely etched away in this region, thus leaving some shunts operational. Note that the removal of the BSF was essential for seeing the inversion channels in the backside LBIC. Similar findings have already been made using EBIC instead of LBIC, where TEM investigations have revealed the existence of SiC particles in the inversion layers [16]. Since the observed inversion channels provide a considerable conductivity, their potential height should be of the order of 1 eV. Similar inversion channels, which, however, did not lead to ohmic shunting, have already been observed and described in so-called RGS material [17].

5. Discussion and conclusions

The main question arising from the results shown in the previous chapter is why the strong shunts are also visible in the LBIC. Since shunts are a property of the dark I–V characteristic, and the LBIC is measured under short circuit conditions where the dark current is zero, why we can see these shunts in the LBIC? The reason is that here our short circuit is not a real one, at least not with respect to the position of the light beam, where the photocurrent is generated. Even if the input resistance of the current amplifier were 0 Ω, the path resistance across the emitter, the bulk of the wafer, the metallization, and the wiring may be as large as several Ω. Figure 7 illustrates this situation in a schematic cross-section through an illuminated cell implying a

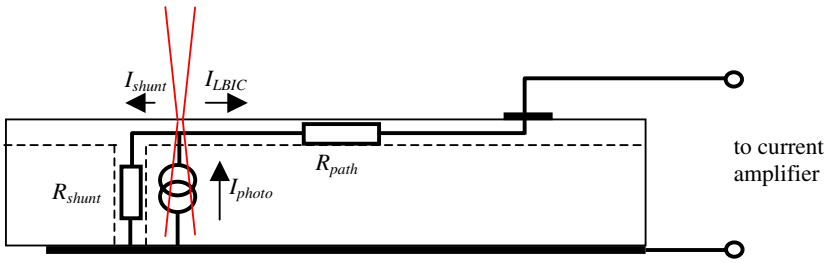

Figure 7. The equivalent circuit of local photocurrent generation near a strong ohmic shunt in a solar cell.

shunt. The light beam and the generation region are indicated, the photocurrent is described by the current source symbol I_{photo}, the shunt is symbolized by the resistance R_{shunt}, and the path resistance by R_{path}. Note that R_{shunt} especially depends strongly on the position of the beam: the more distant the beam is to the shunt position, the larger R_{shunt} becomes. We see that the generated photocurrent divides into two parts, I_{LBIC} flowing to the current amplifier and I_{shunt} flowing across the shunt. If the input resistance of the current amplifier is assumed to be zero, this equivalent circuit leads to an LBIC signal of

$$I_{\text{LBIC}} = I_{\text{photo}} \frac{R_{\text{shunt}}}{R_{\text{path}} + R_{\text{shunt}}}. \tag{1}$$

If the beam is sufficiently distant from the shunt ($R_{\text{shunt}} \gg R_{\text{path}}$) the whole photocurrent flows to the current amplifier. However, if the beam is near the shunt, at least some part of the photocurrent is drained by the shunt, leading to a dark LBIC contrast around sufficiently strong shunts. This model also explains why these dark clouds were not visible in the LBIC image figure 5(c), though also there was a strong ohmic shunt. However, in this case the shunt was not lying between the free emitter and the base as shown in figure 7 but rather between a grid line and the base. Thus, the shunt was lying directly at the input of the current amplifier, where it is inactive since the current amplifier itself has a very low input resistance.

In conclusion, we have shown that LBIC and lock-in IRT provide complementary information to inhomogeneous solar cells. LBIC mainly displays inhomogeneities reducing the short circuit current, which are due to recombination-active defects. Lock-in IRT, on the other hand, allows us to display and investigate inhomogeneities of the dark I–V characteristic, which mainly affects the fill factor and the open circuit voltage of the cell. Since the efficiency of a solar cell is proportional to the product of all these three cell parameters, for optimising the efficiency both techniques can advantageously be applied. It turns out that especially strong ohmic shunts can be observed also by LBIC imaging, if they are not lying below grid lines. We have shown that this contrast mechanism differs from that of recombinative defects. Here it is not the recombination activity of the defect which reduces the photocurrent, but by the action of a resistive current divider only some part of the generated photocurrent reaches the current amplifier. Hence, for shunted solar cells we actually have to regard three LBIC contrast mechanisms: (1) the usual recombination contrast, (2) the shadow contrast of the grid metallization, and (3) the resistive current divider contrast near strong ohmic shunts. LBIC investigations on strongly shunted cells performed from the rear side with the base contact removed have proven indications of the existence of inversion layers crossing the cells along grain boundaries. This type of shunts seems to be the most dangerous material-induced one in multicrystalline solar cells.

Acknowledgment

This work was partly supported by the BMBF project no 0329846D (ASIS).

References

[1] Green M A 1992 *Solar Cells, Operating Principles, Technology, and System Applications* (Kensigton, NSW: University of New South Wales) ISBN 0 85823 580 3
[2] Häßler C, Thurm S, Koch W, Karg D and Pensl G 1995 *13th European Photovoltaic Solar Energy Conf. (France, 1995)* (Bedford, UK: H.S. Stephens and Associates) p 1364
[3] van der Heide A S H, Schönecker A, Wyers G P and Sinke W C 2000 *16th European Photovoltaic Solar Energy Conf. (Glasgow, 2000)* (London, UK: James and James (Science Publishers) Ltd) p 1438
[4] Färber G, Bardos R A, McIntosh K R, Honsberg C B and Sproul A B 1998 *2nd World Conf. on Photovoltaic Solar Energy Conversion (Vienna, Austria, 1998)* (Ispra, Italy: European Commission) p 280
[5] Ballif C, Peters S, Isenberg J, Riepe S and Borchert D 2002 *29th IEEE PVSC (New Orleans, 2002)* (US: IEEE, Library of Congress) p 446
[6] Breitenstein O, Eberhardt W and Iwig K 1994 *1st World Conf. on Photovoltaic Energy Conversion (Hawaii, 1994)* (US: IEEE, Library of Congress) p 1633
[7] Simo A and Martinuzzi S 1990 *21st IEEE PVSC (Kissimee, 1990)* (US: IEEE, Library of Congress) p 800
[8] Kaminski A, Jouglar J, Moreau M, Lombard V, Vuillermoz P L and Laugier A 1998 *Proc. 2nd World Conf. on Photovoltaic Solar Energy Conversion (Vienna, Austria, 1998)* (Ispra, Italy: European Commission) p 2316
[9] Breitenstein O, Langenkamp M, Lang O and Schirrmacher A 2001 *Sol. Energy Mater. Sol. Cells* **65** 55
[10] Breitenstein O and Langenkamp M 1998 *2nd World Conf. on Photovoltaic Solar Energy Conversion (Austria, 1998)* (Ispra, Italy: European Commission) p 1382
[11] Breitenstein O, Rakotoniaina J P, Neve S, Green M A, Zhao J, Wang A and Hahn G 2002 *Proc. 29th IEEE PVSC (New Orleans, 2002)* (US: IEEE, Library of Congress) p 430
[12] Breitenstein O and Langenkamp M 2003 *Lock-in Thermography—Basics and Applications to Functional Diagnostics of Electronics Components* (Heidelberg: Springer) ISBN 3-540-43439-9
[13] Boyeaux J P and Laugier A 1989 *Rev. Phys. Appl.* **24** C6 111
[14] www.thermosensorik.com
[15] Breitenstein O, Rakotoniaina J P, Altmann F, Schulz J and Linse G 2002 *ISTFA 2002: Proc. 28th Int. Symp. for Testing and Failure Analysis (Phoenix, AZ, 2002)* (Materials Park, Ohio: ASM International) p 29
[16] Rakotoniaina J P, Neve S, Werner M and Breitenstein O 2002 *Proc. PV in Europe (Rome, 2002)* (Germany: WIP Munich) p 24
[17] Breitenstein O, Langenkamp M and Rakotoniaina J P 2002 *Solid State Phenom.* **78/79** 29